Estimation of Focal Length Variations of a 100 m Radio Telescope's Main Reflector by Laser Scanner Measurements

Christoph Holst[1], Philipp Zeimetz[2], Axel Nothnagel[3], Wolfgang Schauerte[4], Heiner Kuhlmann[5]

Abstract

Due to gravitation, the main reflector of a radio telescope underlies a deformation which causes a change in focal length depending on the variations of the elevation angle of the telescope. In order to estimate these gravity dependent deformations of the main reflector of the 100 m radio telescope at Effelsberg, Germany, we propose a measurement concept based on a laser scanner being mounted upside-down on the subreflector. The measurements which have been performed at seven different elevations between 90 and 7.5 are used to estimate the focal length variation of the main reflector parameterized by a rotational paraboloid. To guarantee reliability of the adjustment, we perform an orthogonal distance regression (ODR) rather than a classical least squares adjustment in a Gauss-Helmert model. We formulate the independence of the focal length estimation from the absolute position and orientation of the main reflector in space as a requirement for a reliable adjustment approach. Our investigations attest the ODR a superior reliability with regard to this criterion. A three-step adjustment procedure based on an alteration of the ODR and several outlier eliminations is used to determine the variations of the focal length due to gravitation. The estimated focal length decreases by a maximum of 12.6 mm when tilting the reflector from 90 to 7.5 elevation angle. The post-fit discrepancies between the best-fit paraboloid and the reflector's surface are Gaussian distributed within the accuracy of the measurements which supports the assumption of a homologous deformation of the main reflector.

CE Database subject headings: Laser Scanner; Deformation; Radio Telescope; Orthogonal Distance Regression

Holst, C., Zeimetz, P., Nothnagel, A., Schauerte, W., Kuhlmann, H. (2012): Estimation of focal length variations of a 100-m radio telescope's main reflector by laser scanner measurements, J. Surv. Eng., 138 (3), 126-135

[1]M.Sc., Institute of Geodesy and Geoinformation, University of Bonn, 53115 Bonn, Germany. E-mail: holst@igg.uni-bonn.de

[2]Dr.-Ing., Institute of Geodesy and Geoinformation, University of Bonn, 53115 Bonn, Germany. E-mail: zeimetz@igg.uni-bonn.de

[3]PD Dr.-Ing., Institute of Geodesy and Geoinformation, University of Bonn, 53115 Bonn, Germany. E-mail: nothnagel@uni-bonn.de

[4]Dr.-Ing., Institute of Geodesy and Geoinformation, University of Bonn, 53115 Bonn, Germany. E-mail: schauerte@uni-bonn.de

[5]Prof. Dr.-Ing., Institute of Geodesy and Geoinformation, University of Bonn, 53115 Bonn, Germany. E-mail: heiner.kuhlmann@uni-bonn.de

Introduction

In geodetic VLBI applications, radio telescopes are used to perform measurements of differences in signal arrival times to estimate the distance between the reference points of different telescopes. The signal path within the optics of the telescope does not influence the observation if it remains constant, because it is absorbed in the clock corrections during the data analysis (Sarti et al. 2011). But if the focal length of the main reflector and following the signal path underlie a variation between different elevation angles of the main reflector, these focal length variations can impact the VLBI observable to a non negligible extent. This variation influences, among other parameters, the height of the telescope reference point and, as a consequence, the distance between the telescopes (Sovers et al. 1998). Therefore, this variation has to be known as accurately as possible to correct the VLBI geometric delay. The dependence of the signal path on the construction of the main reflector, i.e., its surface, and on the resulting focal length of the reflector is shown in Fig. 1.

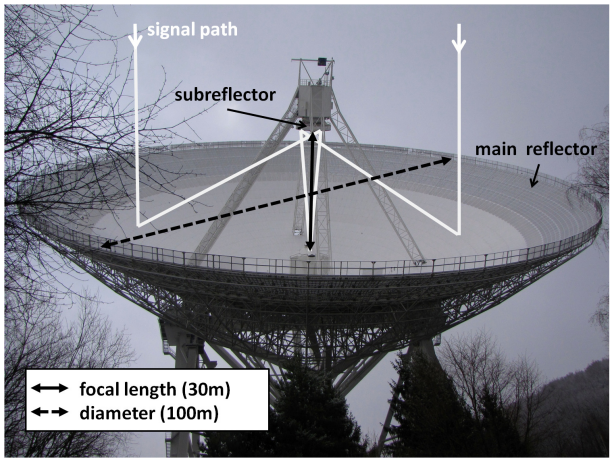

Figure 1: Effelsberg 100 m radio telescope including a sketch of two distinct signal paths.

In general, signal path variations ΔL are not only dependent on the the focal length variation Δf but also on the displacement of the receiver ΔR and the displacement of the main reflector ΔV (Clark and Thomsen 1988). The corresponding equation in dependence of the telescope pointing elevation e is

$$\Delta L(e) = 2 \cdot \alpha_R \cdot \Delta R(e) + \alpha_V \cdot \Delta V(e) + \alpha_f \cdot \Delta f(e). \quad (1)$$

Eq. (1) applies to VLBI systems observing in secondary focus as is the case at the radio telescope of investigation at Effelsberg, Germany. The linear coefficients α_R, α_V and α_f depend on the dimensions and structure of the telescope (Abbondanza and Sarti 2010). Thus, the estimation of focal length variations is only a first, important step towards the definition of a complete correction model for signal path variations due to gravitation (Sarti et al. 2009b). But although not sufficient to determine the total variation of the signal path, knowledge about focal length variations is necessary to define the telescope specific correction model to be implemented in the VLBI data reduction. Nowadays, telescope gravitational deformations, despite their potential impact on the accuracy of VLBI positioning, are neglected in the analysis of geodetic VLBI observations.

In the recent years, many investigations have been done in order to analyze the surface of the main reflector of several radio telescopes. These investigations can be categorized into studies that aimed at measuring the deformations of the main reflector, i.e., its actual shape and surface, and into the studies that aimed at determining the focal length variations of its best-fit approximation and the deformation patterns induced by gravity at different elevation angles. Into the first category, the investigations of Subrahmanyan (2005) and Shankar et al. (2009) can be classified. They used photogrammetric measurements in order to analyze the shape of the main reflector and its smoothness. Also the studies of Dutescu et al. (2009) which are based on laser scanner measurements aimed at determining the shape of the main reflector. They analyzed its deviations from the best-fit surface and the deviation of the actual focal length from the one proposed by the manufacturers at the radio telescope at Wettzell and the Deep Space antenna at Weilheim. The studies of Sarti et al. (2009a) can be included into the second category. They estimated focal length variations of the radio telescopes Medicina and Noto, Italy, in dependence

of the elevation angle based on laser scanner measurements. These investigations are comparable to the ones of our study.

Regarding the aforementioned publications also using a laser scanner for analysis (Dutescu et al. 2009, Sarti et al. 2009a), the measurement conditions coincide in several aspects:

- The main reflectors of the observed radio telescopes are of minor size in diameter (Wettzell: $20\,m$, Weilheim: $30\,m$, Medicina and Noto: $32\,m$) with a focal length of about $10\,m$.
- More than one station had to be occupied by the instrument for the scanning of the whole surface.
- The laser scanner's station was chosen very close to the reflector or even on the surface of the main reflector itself leading to short distance measurements but also to bad angles of incidence.

In order to estimate the gravity dependent deformations of the main reflector of the $100\,m$ radio telescope at Effelsberg, Germany (Fig. 1), we developed a measurement concept which differs in all these aspects. It is optimized for the extremely large size of the reflector and for the surrounding topography which makes it impossible to position the laser scanner outside the radio telescope. Instead, it is mounted upside-down underneath the subreflector near the prime focus (Fig. 2 and 3).

Figure 2: Subreflector of the radio telescope.

Figure 3: Upside-down observing station of the laser scanner inside the subreflector at an elevation angle of 90°of the main reflector.

Because of the main reflector's size of $100\,m$ in diameter and the massive weight of $3'200$ tons of the whole construction (MPIfR 2011), the manufacturers took special care in the design regarding gravita-

tional deformation which is accounted for by a homologous deformation (Hachenberg 1968). This means that the main reflector indeed underlies a gravity dependent deformation but also that the deformed surface always results in a rotational paraboloid again. Thus, only a change in focal length should become noticeable with variable elevation angles and no local deformation patterns should be revealed on the surface (Hachenberg 1968).

Within the adjustment of the observations for the estimation of the focal length, it is essential to choose an appropriate model approach. While Sarti et al. (2009a) apply a classical least squares adjustment in a Gauss-Markov model, Dutescu et al. (2009) compare the estimated parameters of a classical least squares approach in a Gauss-Helmert model with the ones of an adjustment with pseudo observations and a fitting method of the Software Mathematica leading to equal results. As a condition for the verification of a suitable adjustment approach, we formulate that the focal length estimation should be independent from the absolute values of the parameters describing the position and orientation of the main reflector in space. For this purpose, we investigate and compose two distinct approaches, i.e., a classical least squares adjustment in a Gauss-Helmert model and an orthogonal distance regression, which differ in the point of linearization and the definition of the estimated discrepancies.

In summary, two main aspects are contained in this paper: First, the specific mounting of the laser scanner inside the subreflector which leads to its station being temporary upside-down. Second, an advanced adjustment model represented by the orthogonal distance regression is used for parameter estimation. These aspects will be further discussed in the following sections.

Laser Scanner Measurements

In order to estimate the elevation dependent deformations, laser scanner measurements were performed on July 8th, 2010, at seven different elevation angles between 90˚and 7.5˚, i.e., 90˚, 75˚, 60˚, 45˚, 30˚, 15˚, 7.5˚. This represents the maximal range of operation. An observing station outside of the telescope as an absolute static position was not feasible. As a consequence, we mounted the instrument on top of a special receiver box which was hoisted to the prime focus underneath the subreflector (Fig. 2 and 3). That means that the laser scanner moves with the telescope's steel structure for different elevations and that its vertical axis is always pointing approximately into the direction of the main reflector's vertex. This results in scanning distances from $30\,m$ to $50\,m$. Thus, at an elevation angle of 90˚of the radio telescope the standing axis of the laser scanner was upside-down and at an elevation angle of 7.5˚the standing axis was nearly horizontal.

Because of this arrangement, it was possible to scan nearly the whole surface of the main reflector from one laser scanner station. Therefore, the necessity for a matching procedure for separate point clouds from several stations as mentioned in Dutescu et al. (2009) and Sarti et al. (2009a) is avoided. Furthermore, this reduces the complexity of the measurement procedure because no target points had to be installed for transformations as well as it benefits the accuracy because no matching process is performed. Another benefit of this station is the geometry of the measurement leading to angles of incidence of larger than 55.

The observation vector $\mathbf{l}_i = [s_i, \beta_i, t_i]^T, i = 1, ..., m$, of a laser scanner includes the distances s_i, the vertical angles β_i and the horizontal directions t_i. These measurements are related to a fixed interval of horizontal direction increments and vertical angle increments, determined by the desired scan resolution, an the phase-based distance measurements. The measurements can be transformed into the coordinates $\mathbf{X}_i$ by Eq. (2), represented in the coordinate system defined by the origin and the axes of the laser scanner:

$$\mathbf{X}_i = \begin{bmatrix} X_i \\ Y_i \\ Z_i \end{bmatrix} = \begin{bmatrix} s_i \cdot \sin\beta_i \cdot \sin t_i \\ s_i \cdot \sin\beta_i \cdot \cos t_i \\ s_i \cdot \cos\beta_i \end{bmatrix}. \tag{2}$$

Additionally, the laser scanner also measures the intensity of the reflected signal. This normalized intensity $I \in [0, 1]$ can be used to segment the main reflector from the background as will be discussed later.

For the measurements with distances from $30\,m$ to $50\,m$, a Leica HDS 6100 laser scanner was used. The scan density was chosen as Ultra High leading to a density of $7.9\,mm \cdot 7.9\,mm$ at a distance of $50\,m$ (Leica Geosystems 2011). This results in a point cloud of about $m \approx 370$ million points and a measurement time of about 30 minutes for each elevation angle. The associated specifications of accuracy of the laser

Observation	Accuracy
$s \leq 25\,m$	$\leq 2\,mm - 3\,mm$
$s \leq 50\,m$	$\leq 3\,mm - 5\,mm$
t	$125\,\mu rad$
β	$125\,\mu rad$

Table 1: Relevant accuracy specifications of the distance s, horizontal direction t and vertical angle β corresponding to the laser scanner Leica HDS 6100 (Leica Geosystems 2011).

scanner are presented in Tab. 1. We attest the distance measurements a higher accuracy than quoted by the manufacturer based on in-house calibration measurements. These test measurements were performed at different distances with respect to an interferometer of superior accuracy. The standard deviation of $\sigma_{s,i} = 0.6\,mm + s_i \cdot 0.05\,mm/m$ results in an accuracy of $2.1\,mm$ at a distance of $30\,m$ and in $3.1\,mm$ at a distance of $50\,m$. However, because these values are achieved under optimal conditions which are not given during the measurements at the paraboloid, we adopt the specifications of Tab. 1 leading to a standard deviation of the distance measurements of $\sigma_{s,i} = s_i \cdot 0.1\,mm/m$ which equals an accuracy of $3.0\,mm$ at a distance of $30\,m$ and $5.0\,mm$ at a distance of $50\,m$. As described in the final results, an analysis of the post-fit discrepancies supports this magnitude.

Adjustment Approaches

We parameterize the surface of the main reflector by a rotational paraboloid. We choose this representation because of the assumption of a homologous deformation of the surface always leading to a rotational paraboloid again (Hachenberg 1968). The corresponding parameters can be separated in extrinsic parameters describing the position and orientation of the paraboloid in space and in the intrinsic shape parameter, i.e., the focal length. The focal length is the desired parameter to describe the inner deformation caused by a variation at different elevations. Its estimation should be invariant from changes in position and orientation of the main reflector in space. To ensure this requirement, two adjustment approaches are discussed. The first one is based upon a classical least squares minimization and the second one describes two modifications leading to an orthogonal distance regression (ODR).

Parameterization

A rotational paraboloid whose vertex is placed in the origin of the coordinate system and whose rotational axis coincides with the z-axis of the coordinate system is parameterized by

$$\frac{x^2 + y^2}{4f} = z, \tag{3}$$

with f being the focal length as the only intrinsic form parameter (Clark and Thomsen 1988). Because the laser scanner is mounted on the subreflector and not on the vertex of the paraboloid, the measured coordinates $\mathbf{X}$ have to be transformed into the coordinates $\mathbf{x} = [x, y, z]^T$ by a rotation around the x- and y-axis, i.e., φ_x, φ_y, and a translation $\mathbf{x}_v = [x_v, y_v, z_v]^T$ before being related to the focal length by Eq. (3). The rotation around the z-axis is neglected due to the rotational symmetry of the paraboloid. Thus, the implicit model of the rotational paraboloid $g(\mathbf{X}, \mathbf{p}) = \mathbf{0}$, expressed in the measured coordinates $\mathbf{X}$, is defined by six parameters $\mathbf{p} = [x_v, y_v, z_v, \varphi_x, \varphi_y, f]^T$:

$$g: \; g(\mathbf{X}_i, \mathbf{p}) = \frac{x_i^2 + y_i^2}{4f} - z_i = 0. \tag{4}$$

With the definition of the matrices $\mathbf{R}_x(\varphi_x)$ and $\mathbf{R}_y(\varphi_y)$ describing the rotations around the x- and y-axis, the observed coordinates $\mathbf{X}_i$ are transformed into the coordinates $\mathbf{x}_i$ within the laser scanner system by

$$\mathbf{x}_i = \mathbf{R}_x(\varphi_x) \cdot \mathbf{R}_y(\varphi_y) \cdot \mathbf{X}_i - \mathbf{x}_v. \tag{5}$$

As already described, a reliable adjustment of these six parameters enables an estimation of the focal length f independent from the absolute values of the five extrinsic parameters. Therefore, two different adjustment strategies will be discussed in regard to this requirement.

Classical Least Squares Approach

At first, we briefly describe the classical least squares approach because we later refer the improvement of the ODR to this. The classical least squares adjustment is based on an adjustment of the observations $\mathbf{l}$ that can be included into the functional model of Eq. (4) by Eq. (2). Due to the fact that an isolation of the observations in Eq. (4) is impossible, the functional model $g(\mathbf{l}, \mathbf{p}) = \mathbf{0}$ is implicit. This type of least squares adjustment is known as a Gauss-Helmert model or the general case of adjustment (e.g., Mikhail and Ackermann 1976).

While the functional model is given by Eq. (4), the corresponding stochastic model $\Sigma_{\mathbf{ll}}$ rests upon the variances of the measured distance $\sigma^2_{s,i} = s_i^2 \cdot 0.1^2\, mm^2/m^2$, the vertical angle $\sigma^2_{\beta,i} = 125^2\, \mu rad^2$ and the horizontal direction $\sigma^2_{t,i} = 125^2\, \mu rad^2$. As already described, these stochastic informations are extracted from the manufacturer's specifications (see Tab. 1). The combined stochastic model of the observations is a covariance matrix with values only in the main diagonal neglecting correlations:

$$\Sigma_{\mathbf{ll},i} = \mathrm{diag}\{\sigma^2_{s,i}, \sigma^2_{\beta,i}, \sigma^2_{t,i}\}. \tag{6}$$

Because the observations $\mathbf{l}$ are never free of error, i.e., the variances in Eq. (6) are non-zero, residuals $\mathbf{v}$ have to be added in order to gain the estimated observations $\widehat{\mathbf{l}} = \mathbf{l} + \mathbf{v}$ and to fulfill Eq. (4) with the included estimated parameters $\widehat{\mathbf{p}} : g(\widehat{\mathbf{l}}, \widehat{\mathbf{p}}) = \mathbf{0}$. For linearization, the discrepancies $\mathbf{w}$, a design matrix $\mathbf{A}$ and a condition matrix $\mathbf{B}$ have to be set up (e.g., Mikhail and Ackermann 1976). The discrepancies $\mathbf{w}$ represent the deviations between the assumed functional model of Eq. (4), including the observations $\mathbf{l}$ and the approximated parameters $\mathbf{p}_0$, and the best-fit paraboloid:

$$\mathbf{w} = g(\mathbf{l}, \mathbf{p}_0). \tag{7}$$

Through a linearization of the functional model at the approximated parameters $\mathbf{p}_0$ and at the observations $\mathbf{l}$, the design matrix $\mathbf{A}$ and the condition matrix $\mathbf{B}$ are calculated:

$$\mathbf{A} = \left.\frac{\partial g}{\partial \mathbf{p}}\right|_{\mathbf{p}_0,\mathbf{l}}; \qquad \mathbf{B} = \left.\frac{\partial g}{\partial \mathbf{l}}\right|_{\mathbf{p}_0,\mathbf{l}}. \tag{8}$$

By means of the definitions of Eqs. (7) and (8) and the determination of $\Delta\widehat{\mathbf{p}} = \widehat{\mathbf{p}} - \mathbf{p}_0$ as the vector of reduced parameters, it is possible to set up the linearized functional model as

$$\mathbf{B}\mathbf{v} + \mathbf{A}\Delta\widehat{\mathbf{p}} + \mathbf{w} = \mathbf{0}. \tag{9}$$

These definitions form the classical adjustment approach based on a non-linear implicit functional model where the iteration is only performed on the parameters, not on the observations. It is described in several publications, e.g., Kupferer (2004) or Lösler (2009), or standard literature for parameter adjustment, e.g., Mikhail and Ackermann (1976) or Niemeier (2008).

The estimation of the desired parameters $\widehat{\mathbf{p}}$ is then based upon the minimization of the cost function $\mathbf{v}^T\Sigma_{\mathbf{ll}}^{-1}\mathbf{v}$ which leads to the normal equations (Mikhail and Ackermann 1976)

$$\begin{bmatrix} \mathbf{B}\Sigma_{\mathbf{ll}}\mathbf{B}^T & \mathbf{A} \\ \mathbf{A}^T & \mathbf{0} \end{bmatrix} \begin{bmatrix} \mathbf{k} \\ \Delta\widehat{\mathbf{p}} \end{bmatrix} = \begin{bmatrix} -\mathbf{w} \\ \mathbf{0} \end{bmatrix}, \tag{10}$$

where $\mathbf{k}$ are the Lagrange multipliers. By solving this equation system, the reduced parameters $\Delta\widehat{\mathbf{p}}$ and following $\widehat{\mathbf{p}} = \mathbf{p}_0 + \Delta\widehat{\mathbf{p}}$ and the associated covariance matrix $\Sigma_{\widehat{\mathbf{p}}\widehat{\mathbf{p}}}$ can be estimated iteratively.

Orthogonal Distance Regression

The described approach of the classical least squares adjustment is not an optimal solution for estimation of the parameters $\widehat{\mathbf{p}}$ of the implicit model of Eq. (4). This is based on two reasons:

- First, the design matrix $\mathbf{A}$ and the condition matrix $\mathbf{B}$ are not linearized at the paraboloid itself represented by the estimated observations $\widehat{\mathbf{l}} = \mathbf{l} + \mathbf{v}$ but at the true observations $\mathbf{l}$ (Eq. (8)).
- Second, an algebraic error criterion as stated in Eq. (7) is used to define the discrepancies instead of a geometrically interpretable one.

The orthogonal distance regression (ODR) overcomes the drawbacks of the classical least squares adjustment (Ahn et al. 2002).

The first insufficiency is discussed in several geodetic publications (e.g., Lenzmann and Lenzmann 2003, Neitzel 2010). An adaption of the point of linearization can also be found in the actual document about concepts of adjustments of the German Institute for Standardization (DIN 18709, 2010): While in the document of the year 1984 (DIN 18709, 1984) a linearization at the observations $\mathbf{l}$ similar to Eq. (8) is propagated, the document of 2010 suggests a strict linearization at the estimated observations $\widehat{\mathbf{l}}$ in non-linear models. This modification as described in Lenzmann and Lenzmann (2003) and Neitzel (2010) leads to a different definition of the vector of discrepancies. They refer to the associated algorithm as total least squares representing a rigorous solution of the Gauss-Helmert model.

The ODR as a technique for shape recognition and approximation is well known in the mathematics or computer science community (e.g., Helfrich and Zwick 1993, Ahn 2008). While the classical least squares approach is often named as algebraic fitting, the ODR is referred to as geometric fitting being superior in regard to the algebraic one because of the following reasons (Ahn et al. 2001):

- The algebraic fitting has drawbacks in accuracy.
- The estimated intrinsic parameters are invariant to the position and orientation of the shape in space in comparison to the algebraic fitting.
- The geometric discrepancies are physically interpretable. In contrast, the algebraic discrepancies of Eq. (7) do not follow a physical interpretation not being equal to a geometric distance.

To overcome these insufficiencies, the aforementioned modifications have to be accomplished. Because the foundation of this ODR approach is a coordinate-based distance as a criterion for the discrepancies, we directly include the measured points $\mathbf{X}$ into the functional model instead of the observations $\mathbf{l}$ so that the implicit model $g(\mathbf{X}, \mathbf{p}) = \mathbf{0}$ is given as in Eq. (4). The associated stochastic model $\Sigma_{\mathbf{XX}}$ is gained by variance propagation (e.g., Mikhail and Ackermann 1976) of the covariance matrix of the observations $\Sigma_{\mathbf{ll},i}, i = 1, ..., m$, of Eq. (6):

$$\Sigma_{\mathbf{XX},i} = \left[\frac{\partial \mathbf{X}_i}{\partial \mathbf{l}_i}\right] \cdot \Sigma_{\mathbf{ll},i} \cdot \left[\frac{\partial \mathbf{X}_i}{\partial \mathbf{l}_i}\right]^T. \tag{11}$$

In contrast to the stochastic model $\Sigma_{\mathbf{ll},i}$ of the classical least squares approach, the covariance information $\Sigma_{\mathbf{XX},i}$ of the ODR is a full matrix including correlations due to variance propagation.

Helfrich and Zwick (1993) divide the algorithm in two parts: The first one is based upon the calculation of estimated coordinates, i.e., the orthogonal contacting points $\mathbf{X}'$, which lie on the estimated paraboloid parameterized by the actual approximated parameters $\mathbf{p}_0$. They represent the shortest distances, i.e., the signed orthogonal distances, between the measured points $\mathbf{X}$ and the paraboloid $g(\mathbf{X}', \mathbf{p}_0) = \mathbf{0}$ (Fig. 4). These are the correspondents to the estimated observations $\widehat{\mathbf{l}}$ because we now adjust the measured coordinates $\mathbf{X}$ instead of the observations $\mathbf{l}$.

The second part defines signed orthogonal distances $\mathbf{d}$ to set up the discrepancies geometrically. This two-step adjustment as described in Helfrich and Zwick (1993) is also called the separation of variables approach in which the calculation of orthogonal contacting points $\mathbf{X}'$ and the estimation of the optimal parameters $\widehat{\mathbf{p}}$ is separated in an inner and outer iteration until convergence is reached (Rouhani and Sappa 2009).

For the parameter estimation, we preserve the normal equation (Eq. (10)) while we define the required variables, i.e., the matrices $\mathbf{A}$, $\mathbf{B}$ and the discrepancies $\mathbf{w}$, deviant from Eqs. (7) and (8) adjusted to the ODR approach as described below.

We linearize the implicit model $g(\mathbf{X}, \mathbf{p}_0)$ of Eq. (4) including the observed coordinates $\mathbf{X}$ and the approximated parameters $\mathbf{p}_0$ at approximated coordinates $\mathbf{X}_0$ by a Taylor series:

$$\begin{aligned} g(\mathbf{X}, \mathbf{p}_0) = & g(\mathbf{X}_0, \mathbf{p}_0) + \nabla g_{\mathbf{X}_0} \cdot (\mathbf{X} - \mathbf{X}_0) \\ & + O\{(\mathbf{X} - \mathbf{X}_0)^2\}. \end{aligned} \tag{12}$$

The gradient $\nabla g_{\mathbf{X}_0}$ is defined as $\nabla g_{\mathbf{X}_0} = [g_{X_0}, g_{Y_0}, g_{Z_0}]^T$, with $g_{X_0} = \partial g(\mathbf{X}, \mathbf{p}_0)/\partial X_0$ and the terms of higher order equal $O\{(\mathbf{X} - \mathbf{X}_0)^2\}$. Then, by definition that the points of linearization are equal to the orthogonal contacting points, i.e., $\mathbf{X}_0 = \mathbf{X}'$, and with the knowledge that the implicit functional model

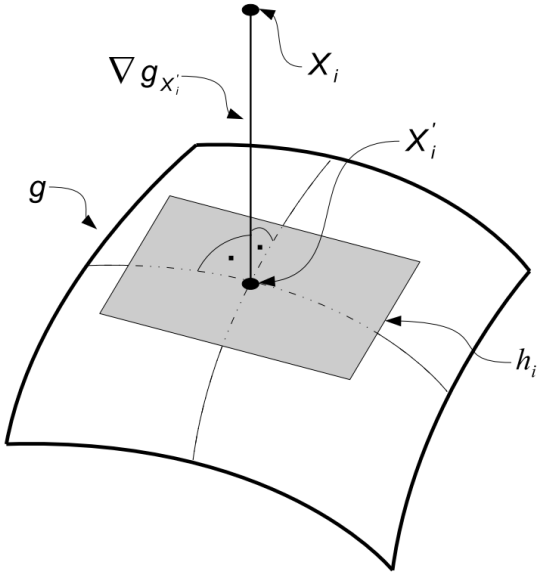

Figure 4: Relation between the measured point $\mathbf{X}_i$ and its correspondent orthogonal contacting point $\mathbf{X}_i'$; the normal vector $\nabla g_{\mathbf{X}_i'}$ is orthogonal to the tangent plane plane h_i which is an approximation of the surface g, i.e., the paraboloid, at $\mathbf{X}_i'$.

equals zero at the orthogonal contacting points $\mathbf{X}'$ lying directly on the paraboloid itself defined by the parameters $\mathbf{p}_0$

$$g(\mathbf{X}', \mathbf{p}_0) = \mathbf{0}, \tag{13}$$

we reduce the linearized Eq. (12) by neglect of the higher order terms to

$$h: \; g(\mathbf{X}, \mathbf{p}_0) = \nabla g_{\mathbf{X}'} \cdot (\mathbf{X} - \mathbf{X}'). \tag{14}$$

Eq. (14) defines tangent planes h, being approximations of the paraboloid g characterized by Eq. (13) at the orthogonal contacting points $\mathbf{X}'$ (Fig. 4). Ahn et al. (2002) describe as necessary condition that the connecting lines of $\mathbf{X}$ and $\mathbf{X}'$ are parallel to the normals of the paraboloid at the points $\mathbf{X}'$ which equal the gradients $\nabla g_{\mathbf{X}'}$:

$$\nabla g_{\mathbf{X}'} \times (\mathbf{X} - \mathbf{X}') = \mathbf{0}. \tag{15}$$

A rearrangement of Eq. (15) leads to (Ahn et al. 2002)

$$\frac{g_{X'}}{X - X'} = \frac{g_{Y'}}{Y - Y'} = \frac{g_{Z'}}{Z - Z'}, \tag{16}$$

which is equal to

$$\left(\mathbf{X} - \mathbf{X}'\right) = \boldsymbol{\lambda} \cdot \nabla g_{\mathbf{X}'}, \tag{17}$$

with some unknown vector $\boldsymbol{\lambda} = [\lambda_1, ..., \lambda_m]^T$. Eqs. (13) and (17) together build up the necessary first order conditions for the calculation of the orthogonal contacting points $\mathbf{X}'$ (Helfrich and Zwick 1993). In order to estimate the corresponding unknown parameters of dimension four for each measured point $\mathbf{X}_i$, i.e., the orthogonal contacting point $\mathbf{X}_i'$ and the scalar λ_i, $i = 1, ..., m$, we solve this four dimensional equation system iteratively. Therefore, we integrate Eq. (17) into Eq. (14). This results in the calculation of the vector $\boldsymbol{\lambda}$

$$\boldsymbol{\lambda} = \frac{g(\mathbf{X}, \mathbf{p}_0)}{||\nabla g_{\mathbf{X}'}||^2}, \tag{18}$$

whereupon the squared normalization factor of the orthogonal contacting points, $||\nabla g_{\mathbf{X}'}||^2 = g_{X'}^2 + g_{Y'}^2 + g_{Z'}^2$, is iteratively updated by an isolation of the orthogonal contacting points $\mathbf{X}'$ in Eq. (17). For initialization, we set $||\nabla g_{\mathbf{X}'}||^2$ equal to $||\nabla g_{\mathbf{X}}||^2$. After a defined convergence criterion is reached, we finally can

recalculate the orthogonal contacting points $\mathbf{X}'$ by Eq. (17) so that the design matrix and the condition matrix end up as

$$\mathbf{A} = \left.\frac{\partial g}{\partial \mathbf{p}}\right|_{\mathbf{p}_0,\mathbf{X}'}; \quad \mathbf{B} = \left.\frac{\partial g}{\partial \mathbf{X}}\right|_{\mathbf{p}_0,\mathbf{X}'}, \tag{19}$$

linearized at the approximated parameters $\mathbf{p}_0$ as well as at the approximated coordinates, i.e., the orthogonal contacting points $\mathbf{X}'$. This inner iteration is performed at each outer iteration step for the estimation of the parameter update $\Delta\widehat{\mathbf{p}}$.

For the calculation of the signed orthogonal distance in the outer iteration, we build up the Hessian normal form of the planes h by normalizing Eq. (14) with the normal vectors' length $||\nabla g_{\mathbf{X}'}||$:

$$\frac{\nabla g_{\mathbf{X}'}}{||\nabla g_{\mathbf{X}'}||} \cdot (\mathbf{X} - \mathbf{X}') - \frac{g(\mathbf{X}, \mathbf{p}_0)}{||\nabla g_{\mathbf{X}'}||} = \mathbf{0}. \tag{20}$$

The signed distances $\mathbf{d}$ from points $\mathbf{X}$ to their closest points $\mathbf{X}'$ lying on approximated planes can be defined by $\mathbf{d} = \nabla g_{\mathbf{X}'}/||\nabla g_{\mathbf{X}'}|| \cdot (\mathbf{X} - \mathbf{X}')$ with $\nabla g_{\mathbf{X}'}/||\nabla g_{\mathbf{X}'}||$ being the unit normal vectors of the planes (e.g., Hoppe et al. 1992). Because we equalize the signed distances $\mathbf{d}$ with the discrepancies of the adjustment $\mathbf{w}$, we define the discrepancies of the ODR based upon Eq. (20) as

$$\mathbf{w} = \frac{g(\mathbf{X}, \mathbf{p}_0)}{||\nabla g_{\mathbf{X}'}||}. \tag{21}$$

With the definition of the design and condition matrices of Eq. (19) and the discrepancies of Eq. (21), we build up the normal equation (Eq. (10)) and estimate the parameters $\widehat{\mathbf{p}}$ and the associated covariance matrix $\Sigma_{\widehat{\mathbf{p}}\widehat{\mathbf{p}}}$ iteratively analogue to the classical least squares approach. Instead of using $\Sigma_{\mathbf{ll}}$ of Eq. (6) as stochastic model, now $\Sigma_{\mathbf{XX}}$ of Eq. (11) is included into the normal equations as already mentioned.

Helfrich and Zwick (1995, 1996) propose a trust region algorithm for the iterative adjustment. Here, the size of the iteratively estimated reduced parameters $\Delta\widehat{\mathbf{p}}$ is limited as in the Levenberg-Marquardt algorithm (e.g., Moré 1978). But in addition, this limitation factor is adjusted in every iteration step by a defined neighborhood. We neglect an adaption of this extension in the presented application because of reliable initial approximate values $\mathbf{p}_0$ which ensure the convergence. We gain these initial values by the knowledge about the approximate focal length and the spatial transformation between the main reflector and the subreflector. These parameters are sufficient due to the fact that the laser scanner is mounted on the subreflector with its vertical axis approximately pointing into the direction of the main reflector's vertex.

The formulation of the discrepancies in Eq. (21) is comparable to the one discussed by, e.g., Sampson (1982): $\mathbf{w} = g(\mathbf{X}, \mathbf{p}_0)/||\nabla g_{\mathbf{X}}||$. Here, the discrepancies are also normalized but not with the gradient at the point of the orthogonal contacting points $\mathbf{X}'$ but directly at the measured coordinates $\mathbf{X}$. This is a simplification of the approach used here without the need of calculating the orthogonal contacting points (Martínez-Morera and Sarlabous 2003). Several publications, e.g., Ahn et al. (2002), call this approach of the normalized algebraic distance fitting superior to the classical least squares fitting but inferior to the geometric fitting of the ODR.

Comparison of Approaches

A reliable estimation of the focal length is independent from the absolute values of the position and orientation of the rotational paraboloid in space (Ahn et al. 2002). In order to proof the stability of the focal length estimation in regard to this requirement, we transform the point clouds representing the main reflector. Therefore, we change the zero direction of the measured horizontal direction t_i of the observations iteratively by

$$\widetilde{t}_{i,j} = t_i + \frac{2\pi}{k} \cdot j, \tag{22}$$

with $j = 1, ..., k$ steps so that $\widetilde{t}_{i,k} = t_i$. This produces a horizontal rotation of the main reflector inside the laser scanner coordinate system (X_i, Y_i, Z_i). This equals a transformation of four parameters in the paraboloid coordinate system (x_i, y_i, z_i), i.e., a rotation around the φ_x- and φ_y-angles and a translation in x- and y-direction named x_v and y_v. Thus, as a result of the adjustment approaches with input

Elevation []	CLS $[mm]$	ODR $[mm]$
90	0.2	0.0
75	0.1	0.0
60	0.6	0.0
45	0.8	0.0
30	0.5	0.0
15	0.9	0.0
7.5	1.7	0.0

Table 2: Maximal variation of the parameters $\widetilde{f}_j$ due to an alteration of the horizontal direction $\widetilde{t}_{i,j}$ as stated in Eq. (22). The adjustment is performed within a classical least squares approach (CLS) and the orthogonal distance regression (ODR).

of the rotated observations $\widetilde{\mathbf{l}}_{i,j} = [s_i, \beta_i, \widetilde{t}_{i,j}]^T$ or the rotated point clouds $\widetilde{\mathbf{X}}_{i,j}$ calculated by Eq. (2), respectively, only these four parameters $\widetilde{x}_{v,j}$, $\widetilde{y}_{v,j}$, $\widetilde{\varphi}_{x,j}$ and $\widetilde{\varphi}_{y,j}$ should underly a variation with altering j. In contrast, the estimated translation in z-direction $\widetilde{z}_{v,j}$ and the estimated focal length $\widetilde{f}_j$ should remain constant for all $j = 1, ..., k$.

An analysis of the different point clouds of the varying elevations results in six parameters per each of the seven elevations per k steps. In order to make a reliable conclusion, we chose a number of $k = 36$ steps which equals 10 as step size.

As a result, the curves of the estimated transformation dependent parameters $\widetilde{x}_{v,j}$, $\widetilde{y}_{v,j}$, $\widetilde{\varphi}_{x,j}$ and $\widetilde{\varphi}_{y,j}$ (not shown here) match in magnitude and form between the classical least squares approach and the ODR. The largest deviations between the two adjustment procedures are about $1.8\,mm$ concerning the two estimated translations $\widetilde{x}_{v,j}$ and $\widetilde{y}_{v,j}$. The superior reliability of the ODR over the classical least squares adjustment is revealed by an analysis of the estimated focal lengths $\widetilde{f}_j$: while they stay constant within the ODR, they vary significantly within the classical least squares approach. The variations of the classical least squares approach always follow a sine curve with varying magnitude and location of local maximum (Fig. 5). The results of maximal parameter variation $\widetilde{f}_j$ are presented in Tab. 2. As can be seen, the variation corresponding to the classical least squares approach is maximal at an elevation of 7.5 and minimal at 75 elevation, whereas the maximal variations corresponding to the ODR always stay zero regarding the accuracy of calculation.

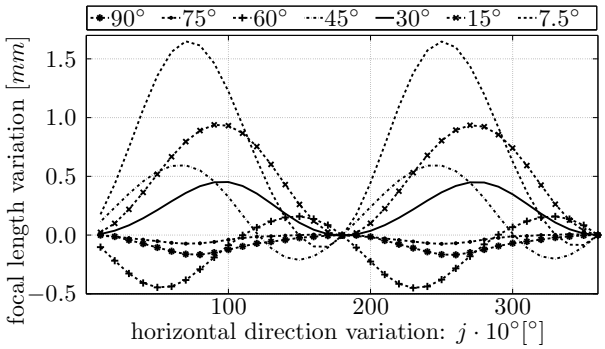

Figure 5: Reduced relative variation of the estimated focal length $\widetilde{f}_j$ within the classical least squares approach due to a change in horizontal direction as stated in Eq. (22).

These results attest the ODR approach a superior performance over the classical least squares approach with regard to the requirement of a reliable focal length estimation independent from changes in position and orientation of the observed main reflector of the radio telescope in space. Thus, in order to guarantee a focal length estimation as accurately as possible, we choose the ODR for parameter estimation within the whole data processing procedure presented in the next section.

Data Processing and Results

For data processing, we propose a stepwise adjustment procedure consisting of the ODR and outlier eliminations. We first describe this stepwise adjustment procedure before we illustrate the final results of the deformation analysis with regard to the focal length variation due to gravitation.

Stepwise Adjustment Procedure

As already described, the measurements at each elevation angle consist of about $m \approx 370$ million points. In order to estimate the focal length based upon each point cloud, the covariance matrix and the Jacobian matrices of Eqs. (11) and (19) have to be built up. Since neighboring data points are highly correlated and processing time has to be optimized, data reduction is performed to an average point spacing of $0.25\,m \cdot 0.25\,m$ which equals a remaining point cloud of $m \approx 1$ million points. We regard this amount of points as sufficient for a reliable parameter estimation because tests show that the parameter estimation is independent from this reduction step. This point cloud reduction step is performed within the Leica Geosystems Software Cyclone. Subsequently, we divide the data processing into three adjustment steps:

- First, the observations of the main reflector are separated from the background by an elimination of all points having a distance from the laser scanner of more than $51\,m$ or less than $30\,m$. These values arise from the geometry of the main reflector and its associated focal length. Additionally, points are eliminated by a threshold in the measured intensity. Therefore, all points having a normalized intensity $I \in [0, 1]$ of $I \leq 0.5$ are excluded. This threshold is set up by an empirical and visual examination.
- After a first parameter estimation within the ODR, systematic outliers are removed from the point cloud by an analysis of the estimated discrepancies $\mathbf{w}$ and a threshold of $5\,cm$. These outliers correspond to the construction of the radio telescope, e.g., the beams of the subreflector, but do not directly lie on the surface of the main reflector.
- The successive second adjustment is followed by a removal of points lying near the edge of the reflector and by an elimination of points with a systematic discrepancy belonging to the construction once again. The points which are lying near the edge are eliminated due to the fact that the outer ring of the main reflector is perforated as can be seen in Fig. 6. Because this perforation produces a partial transparency, the distance measurements of the laser scanner can underlie gross errors influencing the parameter estimation. Afterwards, the final third ODR is performed.

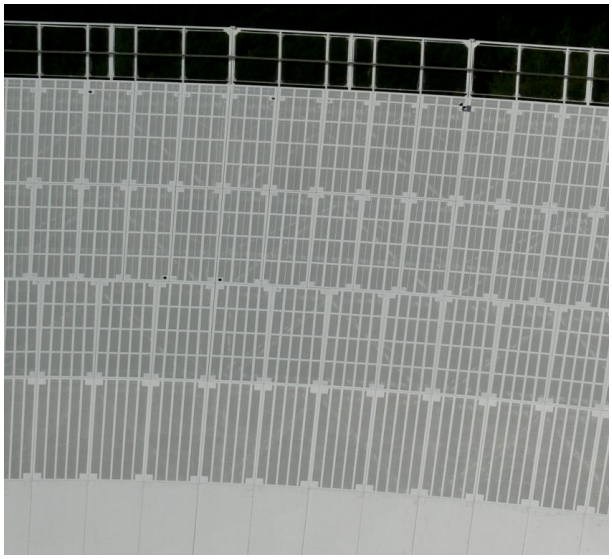

Figure 6: Perforated outer ring of the main reflector. Its radial dimension is approximately $10\,m$.

The resulting point clouds being finally adjusted consist of about $m \approx 500'000$ remaining points. This three-step adjustment procedure is performed within each of the seven point clouds corresponding to the different elevations from 90 to 7.5.

Elevation []	$\widehat{x}_v$ $[m]$	$\widehat{y}_v$ $[m]$	$\widehat{z}_v$ $[m]$	$\widehat{\varphi}_x$ $[rad]$	$\widehat{\varphi}_y$ $[rad]$
90	-0.0467	0.0171	-29.9088	3.1384	0.0094
75	-0.0652	-0.0187	-29.9088	3.1410	0.0106
60	-0.0784	-0.0490	-29.9081	3.1431	0.0113
45	-0.0896	-0.0790	-29.9070	3.1451	0.0121
30	-0.0992	-0.0976	-29.9056	3.1465	0.0126
15	-0.1035	-0.1087	-29.9040	3.1475	0.0130
7.5	-0.1051	-0.1064	-29.9034	3.1475	0.0131

Table 3: Final estimated extrinsic parameters. The standard deviations $\widehat{\sigma}_{x,v} = 0.25\,mm$, $\widehat{\sigma}_{y,v} = 0.25\,mm$, $\widehat{\sigma}_{z,v} = 0.01\,mm$, $\widehat{\sigma}_{\varphi,x} = 0.01\,mrad$ and $\widehat{\sigma}_{\varphi,y} = 0.01\,mrad$ are estimated too optimistic because of the neglect of correlations in the stochastic model of the adjustment.

Elevation []	x' $[mm]$	y' $[mm]$	z $[mm]$
90	0	0	0
75	-3.7	-40.1	-0.0
60	-4.6	-73.1	-0.7
45	-3.8	-105.2	-1.8
30	-5.7	-126.0	-3.2
15	-5.5	-137.9	-4.8
7.5	-7.9	-136.4	-5.4

Table 4: Relative deformation in the spatial relation between the subreflector and the main reflector at the individual elevations. The x'-axis is parallel to the elevation axis of the main reflector, the y'-axis is the main tilting direction and the z-axis equals the rotational axis of the paraboloid.

Final Results

As the final results of the data processing, we obtain six estimated parameters $\widehat{\mathbf{p}}$ for each of the seven elevations with corresponding covariance matrices $\Sigma_{\widehat{\mathbf{p}}\widehat{\mathbf{p}}}$. In Tab. 3, the extrinsic parameters for the seven elevations are given. The associated standard deviations are $\widehat{\sigma}_{x,v} = 0.25\,mm$, $\widehat{\sigma}_{y,v} = 0.25\,mm$, $\widehat{\sigma}_{z,v} = 0.01\,mm$, $\widehat{\sigma}_{\varphi,x} = 0.01\,mrad$, $\widehat{\sigma}_{\varphi,y} = 0.01\,mrad$. These standard deviations do not change significantly between the different elevations. Because of the extremely large number of observations and because of the neglect of spatial correlations between neighboring points, these standard deviations are estimated much too optimistic but a realistic guess is not possible at the moment.

The variations of the extrinsic parameters describe a change in relative position and orientation between the laser scanner and the paraboloid. Because the laser scanner was mounted on the subreflector, the variations reveal a deformation in the spatial relation between main reflector and subreflector. By an integration of the laser scanner station $\mathbf{X}_{LS}$ inside the laser scanner coordinate system, i.e., $\mathbf{X}_{LS} = [0, 0, 0]^T$, into the transformation equation (Eq. (5)), it is possible to calculate the position of the laser scanner $\mathbf{x}_{LS}$ in each paraboloid's coordinate system corresponding to the different elevations. After rotation of the paraboloid's coordinate system around its z-axis so that the x'-axis is roughly parallel to the elevation axis of the telescope and the y'-axis is perpendicular to the $x'z$-plane pointing towards the direction of the tilting of the main reflector, the main direction of this relative deformation can be analyzed. The resulting spatial deformations between main reflector and subreflector are shown in Tab. 4. As can be seen, the main deformation is revealed along the y'-axis, i.e., the vertical tilting direction of the main reflector. The relative deformations in horizontal x'-direction and along the z-axis are of minor size. This effect of relative deformation between main reflector and subreflector originates from two facts: (a) the support beams of the subreflector are independent from the construction of the main reflector and (b) the beams holding the subreflector cabin deform.

It should be emphasized that the determination of the extrinsic parameters in Tab. 3 and the determination of relative spatial deformations in Tab. 4 are purely based upon the adjustments of the individual paraboloid point clouds. For this reason, there is, at this point, no direct and absolute relationship between the location parameters of the individual elevations. The reason is that we do not yet have any link to an absolute reference which would enable us to determine the absolute movements of the

Elevation []	$\widehat{f}$ $[m]$	$\Delta\widehat{f}$ $[m]$
90	29.9892	0
75	29.9880	-0.0012
60	29.9847	-0.0045
45	29.9822	-0.0070
30	29.9794	-0.0098
15	29.9766	-0.0126
7.5	29.9779	-0.0113

Table 5: Final estimated focal length $\widehat{f}$ and its corresponding variation $\Delta\widehat{f}$ (compared to the estimation at 90 elevation). The standard deviations $\widehat{\sigma}_f = 0.05\,mm$ and $\widehat{\sigma}_{\Delta f} = 0.07\,mm$ are estimated too optimistic because of the neglect of correlations in the stochastic model of the adjustment.

paraboloid and the subreflector cabin. These have to be expected due to the homologous construction characteristics of the telescope. Therefore, only the focal length can be considered as a parameter which can be interpreted geometrically between the different elevations.

The focal length $\widehat{f}$ estimated at different elevations is shown in Tab. 5. The associated graph in Fig. 7 reveals a linear decrease of the focal length together with the elevation. An exception is the focal length estimated at the elevation of 7.5 for which the expected strong monotony is violated. However, at this time we cannot yet present a plausible reason for this behavior. The corresponding standard deviation of $\widehat{\sigma}_f = 0.05\,mm$ which does not change significantly between the elevations analogue to the ones of the extrinsic parameters is also estimated too optimistic as already stated above for the extrinsic parameters. As can be seen in Tab. 4, the variation of the focal length $\Delta\widehat{f}$ has a magnitude of $\max\{\Delta\widehat{f}\} = 12.6\,mm$ with a standard deviation of $\widehat{\sigma}_{\Delta f} = 0.07\,mm$, calculated by variance propagation. These significant focal length variations affect the VLBI measurements. The impact of focal length variations on signal path variations as stated in Eq. (1) is further described in Abbondanza and Sarti (2010) and Sarti et al. (2009b, 2011).

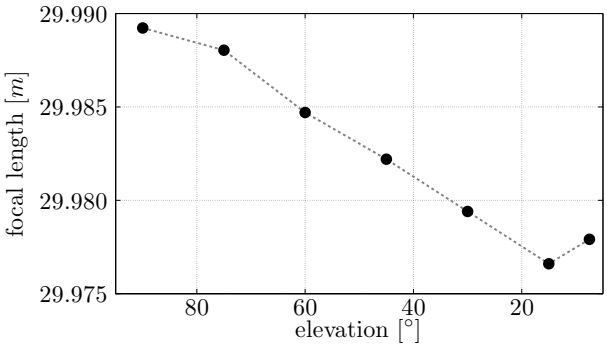

Figure 7: Final estimated focal length $\widehat{f}$ at different elevations.

In order to characterize the quality of the measurements and of the adjustment model, a histogram of the discrepancies of the final best-fit paraboloid of elevation 15 is shown in Fig. 8. The discrepancies follow approximately a Gaussian distribution with a standard deviation of $\widehat{\sigma}_{\mathbf{w}} = 3.2\,mm$. This distribution is similar also for the ones estimated at the other elevations. This empirical standard deviation is very similar to the a priori accuracy of the distance $\sigma_{s,i} = s_i \cdot 0.1\,mm/m$, being between $3\,mm$ and $4\,mm$ at distances between $30\,m$ and $40\,m$ after elimination of the points lying on the perforated outer ring of the main reflector. This consistence supports the magnitude of the a priori accuracy of the distance measurements. This is based on the symmetry of the paraboloid and on the observing station of the laser scanner because it is mounted on the subreflector with its vertical axis pointing approximately into the direction of the main reflector's vertex. Thus, especially the accuracy of the horizontal direction measurements has only a small impact on the parameter estimation whereas particularly the one of the distance measurements is of greater importance.

The discrepancies in the paraboloid's coordinate system of elevation 15 are shown in Fig. 9. On the surface of the main reflector, no significant systematic discrepancies occur within the measurement

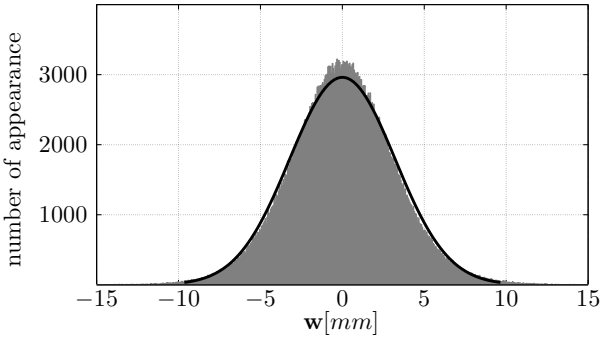

Figure 8: Histogram of the post-fit discrepancies between the best-fit paraboloid and the measured coordinates corresponding to an elevation of 15 (gray), approximated by a Gaussian distribution (black).

accuracy. There are no systematic residuals visible which would lead to the supposition that the observed main reflector would be parameterized better by a surface deviant from a rotational paraboloid. Similar results are obtained for the post-fit discrepancies belonging to the other elevation angles. Thus, no local deformation patterns are revealed. This fact strengthens the assumption of a homologous deformation of the main reflector as stated in Hachenberg (1968).

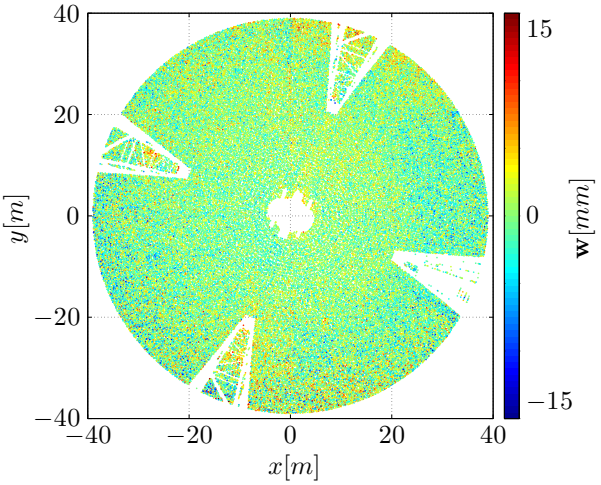

Figure 9: Scatter plot of the post-fit discrepancies **w** between the best-fit paraboloid and the measured coordinates **X** corresponding to an elevation of 15, shown in the paraboloid's coordinate system.

Discussion and Conclusions

In this paper, we present a survey concept and an adjustment procedure that are suitable to estimate the elevation dependent focal length variations of a large paraboloid's main reflector. It consists on the one side on a laser scanner which is mounted on the subreflector so that its station is temporary upside-down. On the other side, the orthogonal distance regression (ODR) is chosen for parameter estimation in order to guarantee unbiased parameter estimates.

Especially the use of a laser scanner proves to be adequate in order to scan a large surface in a comparatively short time with a small spatial discretization in comparison to other geodetic instruments. The adjustment concept with the discussed ODR for parameter estimation enables a reliable estimation of the focal length. The ODR described here is a two-step modification of a classical least squares approach leading to an independence of the focal length estimation from the absolute values of the extrinsic parameters describing the position and orientation of the paraboloid in space.

The adjustment procedure is performed at seven different elevations revealing a significant gravity

dependent decrease of the focal length with a magnitude of $\max\{\Delta\widehat{f}\} = 12.6\,mm$ between 90 and 15 elevation. This decrease is approximately linear disregarding the estimated focal length at an elevation of 7.5. The estimated decrease of focal length as well as the linear characteristic differ from the results in Sarti et al. (2009a) where a greater magnitude was revealed with a quadratic characteristic although their observed reflectors are of smaller size. This different deformation characteristic can be explained by the special construction of the Effelsberg radio telescope leading to a homologous deformation of the main reflector (Hachenberg 1968). This homologous deformation can be confirmed by an analysis of the post-fit discrepancies following a Gaussian distribution. Thus, no local deformation patterns can be revealed inside the surface of the main reflector within the measurement noise which would lead to a best-fit surface deviant from a rotational paraboloid.

It should be emphasized that this study does not offer a detailed quantitative estimation of gravitational deformations of the main reflector. For this purpose, photogrammetric methods, a finite element analysis or other techniques would have been applied. Instead, this study offers a qualitative evaluation of the homologous deformation of the main reflector as well as an estimation of the variability of its focal length. This latter variability is a consequence of the gravitational deformation of the main reflector.

As already mentioned in the introduction, these results only concern one factor of the whole equation which models the signal path variation as described in Clark and Thomsen (1988) (see Eq. (1)). But nevertheless, this estimation of the focal length variation is a first important step towards the definition of a complete correction model of the signal path. Investigations concerning the modeling of the complete correction can be seen in Abbondanza and Sarti (2010) and Sarti et al. (2009b, 2011).

Acknowledgments

We would like to thank Prof. Dr. Hans-Peter Helfrich for his suggestions and discussions regarding the orthogonal distance regression and Ernst-Martin Blome for taking care of the measurements. Additionally, we would like to thank the reviewers for their constructive comments that helped to improve the manuscript.

References

Abbondanza, C. and Sarti, P. (2010). "Effects of illumination functions on the computation of gravity-dependent signal path variation models in primary focus and Cassegrainian VLBI telescopes." *J Geodesy*, 84 (8), 515-525, DOI: 10.1007/s00190-010-0389-z

Ahn, S. J. (2008). "Geometric fitting of parametric curves and surfaces." *Journal of Information Processing Systems*, 4 (4), 153-158, DOI: 10.3745/JIPS.2008.4.4.153

Ahn, S. J., Rauh, W. and Warnecke, H.-J. (2001). "Least-squares orthogonal distances fitting of circle, sphere, ellipse, hyperbola and parabola." *Pattern Recog*, 34 (12), 2283-2303, DOI: 10.1016/S0031-3203(00)00152-7

Ahn, S. J., Rauh, W., Cho, H. S. and Warnecke, H.-J. (2002). "Orthogonal distance fitting of implicit curves and surfaces." *IEEE T Pattern Anal*, 24 (5), 620-638, DOI: 10.1109/34.1000237

Clark, T. A. and Thomsen, P. (1988). "Deformations in VLBI antennas." Nasa Technical Memorandum 100696, NASA, Greenbelt, Md.

DIN 18709 (1984). *Begriffe, Kurzzeichen und Formelzeichen im Vermessungswesen - Teil 4: Ausgleichungsrechnung und Statistik*. Beuth Verlag, Berlin

DIN 18709 (2010). *Concepts, abbreviations and symbols in geodesy - Part 4: Adjustment of observations and statistics*. Beuth Verlag, Berlin

Dutescu, E., Heunecke, O. and Krack, K. (2009). "Formbestimmung bei Radioteleskopen mittels Terrestrischem Laserscanning." *Allgem Verm Nachr*, 6, 239-245

Hachenberg, O. (1968). *Beiträge zur Radioastronomie. Max-Planck-Institut für Radioastronomie Bonn, Studien zur Konstruktion des 100-m-Teleskops*. Band 1, Heft 2, Dümmler, Bonn

Helfrich, H.-P. and Zwick, D. (1993). "A trust region method for implicit orthogonal distance regression." *Numer Algorithms*, 5 (10), 535-545, DOI: 10.1007/BF02108668

Helfrich, H.-P. and Zwick, D. (1995). "Trust region algorithms for the nonlinear least distance problem." *Numer Algorithms*, 9 (1), 171-179, DOI: 10.1007/BF02143933

Helfrich, H.-P. and Zwick, D. (1996). "A trust region algorithm for parametric curve and surface fitting." *J Comput Appl Math*, 73 (1-2), 119-134, DOI: 10.1016/0377-0427(96)00039-8

Hoppe, H., DeRose, T., Duchamp, T., McDonald, J. and Stuetzle, W. (1992). "Surface reconstruction from unorganized points." *Computer Graphics (SIGGRAPH 1992 Proceedings)*, 26 (2), 71-78

Kupferer, S. (2004). "Zur korrekten Linearisierung von nichtlinearen GH-Modellen." *Allgem Verm Nachr*, 11-12, 394-396

Leica Geosystems (2011). "Leica HDS 6100, latest generation of ultra-high speed laser scanner." <www.leica-geosystems.com/hds> (May 11, 2011)

Lenzmann, L. and Lenzmann, E. (2003). "Strenge Auswertung des nichtlinearen Gauß-Helmert-Modells." *Allgem Verm Nachr*, 2, 68-73

Lösler, M. (2009). "New mathematical model for reference point determination of an azimuth-elevation type radio telescope." *J Surv Eng*, 135 (4), 131-135, DOI: 10.1061/(ASCE)SU.1943-5428.0000010

Martínez-Morera, D. and Sarlabous, E. (2003). "On the distance from a point to a quadric surface." *Revista Investigacion Operacional*, 24 (2), 153-161

Mikhail, E. M. and Ackermann, F. (1976). *Observations and least squares.* Dun-Donelly, New York

Moré, J. (1978). "The Levenberg-Marquardt algorithm: implementation and theory." *Numerical Analysis. Lecture Notes in Mathematics 630*, Springer Berlin, Heidelberg, 105-116, DOI: 10.1007/BFb0067700

MPIfR (Max Planck Institute for Radio Astronomy) (2011) "Radio-Observatorium Effelsberg." <http://www.mpifr-bonn.mpg.de/public/eff_d.html> (11.05.2011)

Neitzel, F. (2010). "Generalization of total least-squares on example of unweighted and weighted 2D similarity transformation." *J Geodesy*, 84 (12), 751-762, DOI: 10.1007/s00190-010-0408-0

Niemeier, W. (2008). *Ausgleichungsrechnung. Statistische Auswertemethoden.* 2nd edition, de Gruyter, Berlin, New York

Rouhani, M. and Sappa, A. D. (2009). "A novel approach to geometric fitting of implicit quadrics." *ACIVS, Lect Notes Comput Sc*, 5807, 121-132, DOI: 10.1007/978-3-642-04697-1_12

Sampson, P. D. (1982). "Fitting conic sections to 'very scattered' data: an iterative refinement of the Bookstein algorithm." *Comput Vision Graph*, 18 (1), 97-108, DOI: 10.1016/0146-664X(82)90101-0

Sarti, P., Vittuari, L. and Abbondanza, C. (2009a). "Laser scanner and terrestrial surveying applied to gravitational deformation monitoring of large VLBI telescopes' primary reflector." *J Surv Eng*, 135 (4), 136-148, DOI: 10.1061/(ASCE)SU.1943-5428.0000008

Sarti, P., Abbondanza, C. and Vittuari, L. (2009b). "Gravity-dependent signal path variation in a large VLBI telescope modelled with a combination of surveying methods." *J Geodesy*, 83 (11), 1115-1126, DOI: 10.1007/s00190-009-0331-4

Sarti, P., Abbondanza, C., Petrov, L. and Negusini, M. (2011). "Height bias and scale effect induced by antenna gravitational deformations in geodetic VLBI analysis." *J Geodesy*, 85 (1), 1-8, DOI: 10.1007/s00190-010-0410-6

Shankar, N. U., Duraichelvan, R., Ateequlla, C. M., Nayak, A., Krishnan, A., Yogi, M. K. S., Rao, C. K., Vidyasagar, K., Jain, R., Mathur, P., Govinda, K. V., Rajeev, R. B. and Danabalan, T. L. (2009). "Photogrammetric measurements of a 12-metre preloaded parabolic dish antenna." *Proceedings of the National Workshop on the Design of Antenna and Radar Systems (DARS)*, February 13-14, ISRO Telemetry Tracking and Command Network (ISTRAC), Bangalore, INDIA

Sovers, O. J., Fanselow, J. L. and Jacobs, C. S. (1998). "Astrometry and geodesy with radio interferometry: experiments, models, results." *Rev Mod Phys*, 70 (4), 1393-1454, DOI: 10.1103/RevModPhys.70.1393

Subrahmanyan,R. (2005). "Photogrammetric measurement of the gravity deformation in a cassegrain antenna." *IEEE T Antenn Propag*, 53 (8), 2590- 2596, DOI: 10.1109/TAP.2005.851836